



Fermi National Accelerator Laboratory

FERMILAB-PUB-95-075-T

Complex Systems: Equilibrium Configurations of N Equal Charges on a Sphere ($2 \leq N \leq 112$)

T. Erber

*Department of Physics and Department of Mathematics, Illinois Institute of Technology,
Chicago, Illinois 60616*

G.M. Hockney

*Fermi National Accelerator Laboratory, P.O. Box 500, Batavia, Illinois 60510
(April 18, 1995)*

Abstract

The emergence of complexity in many-body systems is illustrated by the progression of equilibrium states of N charges confined to the surface of a sphere. This is an electrostatic problem with spherically symmetric interactions and boundary conditions. For increasing values of N , the equilibrium solutions break this symmetry and differentiate into sets of complex figures. For instance, states with non-vanishing dipole moments appear when $N = 11, 13, 19$, etc.; the first enantiomeric or chiral state appears at $N = 15$; and robust metastable states are encountered with increasing frequency for $N = 16, 22, 32, 35, 37 \dots$. Computer searches show that when $N \sim 100$, sets of 50-90 metastable states—separated by energy differences of about 0.001%—are the norm. The capture basins, or statistical weights, of some metastable states are larger than those of the ground state. For $N \geq 80$, the energy variations of individual charges *within* configurations exceed the energy differences *between* configurations by factors of 10-50. Angular comparisons show that energetically similar states generally have completely different configurations. Moreover, the geometrical patterns of the charge distributions tend to become increasingly irregular for larger values of N . Nevertheless, there is statistical order in the overall angular distributions, and isolated regular configurations appear at a series of N values extending up to $N = 112$. Since the dipole moments of all known equilibrium states (for $N \leq 112$) are bounded by 10^{-2} , whereas the average dipole moments of spherical random N -point distributions grow as $0.92 N^{\frac{1}{2}}$, it is clear that the geometric irregularity of the Coulomb states coexists with complex order. Common features of the spherical Coulomb and Tammes problems, as well as other cooperative models such as Ewing arrays and vortex lattices, suggest several general conjectures concerning the behavior of complex systems.



1. Introduction

Symmetry and stability criteria are useful for describing charge configurations in a great variety of situations ranging from J.J. Thomson's original plum pudding model of the atom to current investigations of carbon and indium fullerene cages [1-5]. In particular, the $O(4)$ symmetry associated with the Coulomb interaction underlies both the standard Bohr-Pauli level structure of the elements as well the nested charge rings of the old plum pudding model [6-8]. This robust symmetry constraint enabled Thomson to establish the first quantitative connections between recurrences in the patterns of charge distributions and the periodicities of Mendeleyev's chemical table. The most striking recent success of symmetries in charge configurations is the discovery that C_{60} can exist in a stable form resembling a truncated icosahedron [9]. However, since this is the last but one of the 13 Archimedean polyhedra, there are no further regular structures of this kind that can serve as templates for more complex chemical cages. One method of extending the inventory of geometric figures is to use computers to search for the static equilibrium states of N equal point charges on the surface of a sphere. In contrast to the plum pudding or 'jellium' model, where Thomson and Föppl [10] started with the presumption that the equilibrium states would be a series of symmetric nested rings, locally stable solutions of the surface Coulomb problem can be obtained without imposing any *a priori* constraints of symmetry or other types of structural regularities. For small values of N , the results confirm the intuitive expectation that the charge configurations are symmetric and unique. They are also extremely robust because for the special values $N_L = 2 - 6, 12$, the equilibrium configurations remain invariant if the Coulomb law r^{-2} is replaced by the limiting form r^{-n} , $n \rightarrow \infty$ [11]. This 'ultra-repulsive' interaction is the basis of the biological *Tammes* problem of finding arrangements of

N points on the surface of a sphere with the largest possible minimum distance between any pair [12 - 15]. Since exact solutions of the Tammes problem are known for the set $N_T^{ex} = 2 - 12, 24$; this invariance also yields optimum configurations for the surface Coulomb problem for the particular values $N_C^{ex} = 2 - 6, 12$. Of course, these geometric solutions coincide with the computer generated patterns. If the mutual charge repulsions are described by logarithmic interactions rather than a power law, the corresponding equilibrium solutions for $N = 2 - 6, 12$, are again given by the Coulomb set N_C^{ex} [16]. Similar configurations --- except for a few changes in length scales --- appear in the jellium model [10]. All of these equivalences suggest that in cooperative systems with few degrees of freedom symmetry principles alone may be sufficient to determine the character of the equilibrium states. However, when $N > 6$, the sets of equilibrium configurations for these four different force laws lose their resemblance. These divergences illustrate the symmetry breaking effects associated with the emergence of new levels of complexity in larger systems.

In the range $50 \leq N \leq 112$, the surface Coulomb problem has at least 1945 locally stable solutions. These configurations may be classified with the help of several measures based on geometric and energy criteria. Specifically, for any particular value of N, there are a total of $N(N-1)/2$ angles between the \vec{r}_i vectors that specify the locations of the charges on the surface of the sphere. A simple measure of the geometric regularity of a charge distribution is then given by the *angular diversity ratio* (%)

$$D_a(N) \equiv 100 \frac{\text{number of distinct angles}}{N(N-1)/2} . \quad (1.1)$$

Clearly, large values of D_a (percentages exceeding 96% occur frequently when $N > 50$) indicate irregular configurations that cannot be identified with any of the 123 standard types of convex polyhedra [17, 18]. This irregularity also implies that the vertices, or charge positions, of these Coulomb states cannot be interchanged by means of any of the usual rotational symmetry operations. Nevertheless, lack of congruence in vertex separations or edge lengths doesn't exclude the persistence of other kinds of order. A quantitative measure of the difference between random and geometrically irregular distributions of N points on the surface of a sphere is given by the dipole moment or center of charge [19, 20]; i.e.,

$$\vec{d}(N) = \sum_{i=1}^N \vec{r}_i. \quad (1.2a)$$

In particular, for a unit sphere, where $|\vec{r}_i| = 1$, the average value of the dipole moment of a random configuration of N unit charges increases with N ,

$$\langle |\vec{d}(N)| \rangle_{\text{ran}} = \langle |\sum_{i=1}^N \vec{r}_i| \rangle_{\text{ran}} = (\frac{8}{3\pi}N)^{1/2}. \quad (1.2b)$$

On the other hand, the dipole moments of all the equilibrium Coulomb states, for $N \leq 112$, are bounded by 10^2 , and typically fall in the range $10^{-5} \lesssim |\vec{d}(N)| \lesssim 10^{-3}$. Obviously, this is an orders-of-magnitude reduction from the random values. The regularities of the Coulomb states are even more apparent in cases where the angular diversity ratios are small, say $D_a \leq 10\%$. The computer searches show that there are at least 23 geometrically ordered configurations of this kind for a series of N values between $24 \leq N \leq 112$. None of these patterns match the Archimedean polyhedra. For instance, there are four semi-regular Archimedean polyhedra with 24 vertices; and in fact one of them, the snub cube, resembles the ordered Coulomb state with 24 charges because both configurations have 38 faces, 60 edges, and occur in enantiomeric forms. However, all edges of the snub cube have equal length and subtend an angle of 43.68° at the center of the sphere, whereas the 60 edges of the Coulomb configuration are split into three sets with approximately equal lengths: 24 subtending an angle of 42.07° , 24 with an angle of 45.04° , and 12 with an angle of 45.71° . Additional comparisons for other sets of states show that this symmetry breaking is pervasive: there is a general trend away from strict geometric regularity in larger systems.

The emergence of complexity is also reflected in several physical effects. For example, the electrostatic interaction energy of N unit charges, $E(N)$, can be represented as the sum of the partial energies associated with the individual charges, $E_i(N)$; i.e.,

$$E(N) = \sum_{i=1}^N E_i(N); \quad E_i(N) = \frac{1}{2} \sum_{j \neq i}^N |\vec{r}_i - \vec{r}_j|^{-1}. \quad (1.3)$$

This energy sharing is completely symmetric for the equilibrium states of the surface Coulomb problem in small systems; that is, $E_i(N) = E(N)/N$ for $N < 5$. However, when $N = 5$, the equilibrium arrangement is a triangular bipyramid with three charges positioned at the vertices of an equilateral triangle around a great circle, e.g. the equator, and the other two charges at the north and south poles. Since the distances between pairs of equatorial charges exceed the distance from the equator to either pole, Eq. (1.3) implies that each of the two polar charges has a slightly greater partial energy than the equatorial charges. This energy splitting tends to increase for larger values of N ; until at $N = 59$ the state with the greatest capture basin, or statistical weight, is so asymmetric that all of the charges have different partial energies. Beyond this point irregular states with angular diversities at the maximum value $D_a = 100\%$, cf.(1.1), and a complete splitting of all partial energies occur with increasing frequency.

The transition from symmetry to asymmetry also appears in a shift of the center of charge, Eq. (1.2a). For all $N < 11$, the equilibrium configurations of the surface Coulomb problem are sufficiently regular so that the center of charge coincides with the center of the sphere. This situation is analogous to the absence of permanent electric dipole moments in symmetric atomic and molecular charge distributions [21]. But parity arguments alone cannot exclude the existence of dipole moments in static situations. In the surface Coulomb problem this symmetry is broken at $N = 11$, where the equilibrium pattern consists of an irregular equatorial pentagon and two tilted isosceles triangles in the northern and southern hemispheres [22]. This state has a moment given by $|\vec{d}(11)| \approx 0.0132$; which implies the existence of an intrinsic pattern 'direction', as well as a non-vanishing electric field at the center of the sphere.

Another kind of dipole symmetry breaking appears when the charge interactions are varied. For instance, if the Coulomb law is replaced by an $|\vec{r}_i - \vec{r}_j|^{-1}$ force, the dipole moments of all of the corresponding equilibrium configurations vanish identically [16].

A common feature of all three spherical surface problems --- associated with the $|\vec{r}_i - \vec{r}_j|^{-n}$, $n = 1, 2$, and ∞ (Tammes) interactions --- is the occurrence of enantiomeric states beginning at $N = 15$. This division marks another threshold of structural complexity. For example, if computer searches for the equilibrium states of the surface Coulomb problem are started at 10^4 random initial positions of 15 points, the trials will lead with about 50% - 50% probability to two geometrically distinct terminal configurations, $C_G^L(15)$ and $C_G^R(15)$, having precisely the same energy. These pairs of states are labeled 'left' (L) and 'right' (R) because they can be transformed into each other by an improper isometry consisting of a rotation combined with a reflection in a plane perpendicular to the axis of rotation [13]. It is intuitively plausible that there should not be any statistical bias favoring either the 'L' or 'R' states if they are derived from a random mix of initial states by a symmetric process. But in computer simulations the 'L' and 'R' labels may be regarded as a deterministic binary code that can be incorporated into the pseudo-random number algorithms that specify the initial states; and this information can create a preference. Specifically, if $C_{Ram}(15)$ denotes a computer generated initial state of 15 charges, and M is an energy minimizing algorithm, then it can be shown that the mappings $M[C_{Ram}^{L,R}(15)] \rightarrow C_G^{L,R}(15)$ induce a correspondence between the 'L' and 'R' enantiomers of the equilibrium configuration and two disjoint sets of initial states,

$\{C_{Ran}^L(15)\}$ and $\{C_{Ran}^R(15)\}$. These sets of initial states are also enantiomeric because they occur in 'L' and 'R' variants --- each pair related by an improper isometry, and degenerate in energy. In general, the points that make up the initial states are distributed uniformly over the surface of the sphere by sets of pseudo-random number generators. The chirality of the $N = 15$ states then implies that the initial angular coordinates of the charges --- and the corresponding sets of pseudo-random numbers --- can be labeled by a binary 'L' and 'R' alphabet. By choosing appropriate sequences of states it is therefore possible to construct any desired string or 'message' composed of L's and R's. This information, in turn, may be encoded in the pseudo-random number generators by algorithms that retrodict any given sequence [23]. The net effect is that either ground state, $C_G^L(15)$ or $C_G^R(15)$, can be generated by deterministic means although the initial charge configurations are a racemic mix of L and R enantiomers. This method of choice by-passes some of the controversial issues of biological stereochemistry [24, 25].

The equilibrium states of the surface Coulomb problem exhibit many other types of structural transitions. It almost seems as if the addition of every new charge leads to another level of complexity. Basically, this diversity is due to the long range of the Coulomb force: the stable N - body configurations are the result of all $N(N-1)/2$ charge interactions and not just nearest neighbor forces. Similarly, the domain structures and hysteresis of magnetic Ewing arrays arise from the long reach of multipole forces [26]. Finding the stationary states of these cooperative systems by analytical means is generally very difficult. 'Greedy' algorithms that search for global extremals by piecing together a series of local 'best' choices can go astray even in simpler packing and covering problems [27]. For instance, the arrangement of N congruent

spheres whose convex hull has the smallest volume is a straight line or sausage for all $N \leq 56$; but for larger aggregates of spheres the optimum packings have entirely different shapes [28]. In a similar vein, the Tammes problem is equivalent to finding the maximum density — or fraction of covered area — when N congruent spherical caps are packed on the surface of a sphere. Since any cap can touch at most five other caps, this appears to be a nearest neighbor problem with simple contact forces [29]. But the global constraint that all the caps must fit together on the surface of the sphere, in a not necessarily rigid packing, makes this a hard problem. The geometric methods used to construct exact solutions for the set $N_T^{\text{ex}} = 2 - 12, 24$, cannot be extrapolated to algorithms valid for arbitrary N . The best results available for $N \leq 90$ have been obtained by computer searches that simulate the non-overlapping caps with an ultra-repulsive $|\vec{r}_i - \vec{r}_j|^{-n}$, $n = 1, 310, 720$ potential [30]. The surface Coulomb problem is still more complicated because both self-consistent boundary conditions and long range forces determine the extremals. Exact results for this situation are sparse: Topological lower bounds for the number of equilibrium states are known only for $N < 4$ [31]; and local stability has been verified for only a few symmetric ring patterns [32]. Computer studies of this problem are complicated by the existence of many metastable states separated by very small energy differences. In the range $N \leq 112$, this requires double precision computations, high statistics searches starting from many random initial configurations, and numerical stability checks. But even with these precautions some states may be missed; and for large N , roundoff errors affect the correspondence between analytical and numerical stability criteria. These ambiguities are also implicit in computer simulations of the formation of ionic

'crystals' in electromagnetic traps [33, 34], and the relation of protein structures to amino acid sequences [35-37].

Prior work on the surface Coulomb problem, and computer results extending to $N = 65$, are discussed in references [38] and [39]. The values of the ground state energies have meanwhile been confirmed by several independent calculations [40-42, 16]. The Coulomb configurations have a number of practical applications: these include problems in structural chemistry [43, 44], the design of multi-beam laser implosion drives, and the optimum placement of communication satellites. Comprehensive summaries of related packing and covering problems --- with applications to error-free data transmission --- are given in [45]. Some quantum mechanical extensions are discussed in [46-48].

A. Contents

In Section 2A we set up the surface Coulomb problem for N equal point charges, and derive a simple relation between the partial energies associated with the individual charges and the dipole moments of the equilibrium states. The computer algorithms and conventions for orienting the charge configurations are described in Section 2B. Tabulations of the results for the range $2 \leq N \leq 112$ are given in Appendix B. Trends in the number of locally stable states M , found by the computer searches, are summarized in Section 3A. The results indicate an exponential increase in the number of states, i.e., $M \sim \exp \{0.05 N\}$, for $N \geq 50$. Energy relations for the random initial states, ground states, metastable states, and the partial energy distributions within states are discussed in Section 3B. The ground state energies can be represented by a semi-empirical expression of the form $E(N) = 0.5 N^2 - 0.55 N^{3/2}$ over the

entire range $6 < N \leq 112$. Geometric properties of the equilibrium configurations are considered in Section 4: These include the distributions of dipole moments and chiral states in Sections 4A and 4D. Measures of order, such as the angular diversity ratios, and comparisons with Tammes configurations and regular polyhedra are summarized in Section 4B, 4C, and 4E-1. Some general conjectures concerning locally stable states of complex systems are discussed in Section 5. The corresponding analytical and numerical stability criteria are reviewed in Appendix A.

2. The Surface Coulomb Problem

A. Analytic Formulation

The set of N unit vectors $\{\vec{r}_i, 1 \leq i \leq N\}$ describes the position of N point charges constrained to lie on the surface of a unit sphere. If all charges are equal the corresponding dimensionless Coulomb energy is

$$E(N) = \sum_{i=1}^N \sum_{j>i}^N |\vec{r}_i - \vec{r}_j|^{-1}. \quad (2.1)$$

The static equilibrium configurations of this system are specified by the requirement that the total force \vec{F}_i acting on the i^{th} charge is parallel to \vec{r}_i . This condition implies

$$\vec{F}_i = \sum_{\substack{j=1 \\ j \neq i}}^N \frac{\vec{r}_i - \vec{r}_j}{|\vec{r}_i - \vec{r}_j|^3} = E_i(N) \vec{r}_i, \quad (2.2)$$

where $E_i(N)$ is the partial energy associated with the i^{th} charge, cf. (1.3). The equilibrium states of the surface Coulomb problem are special cases of the central configurations of the (non-relativistic) gravitational N-body problem [49-51]. Clearly, the total force on the sphere vanishes

$$\sum_{i=1}^N \vec{F}_i = \sum_{i=1}^N \sum_{j=1, j \neq i}^N \frac{\vec{r}_i - \vec{r}_j}{|\vec{r}_i - \vec{r}_j|^3} = \sum_{i=1}^N E_i(N) \vec{r}_i = 0 \quad (2.3)$$

because the double sum is odd under an interchange of indices. If all the partial energies are equal, i.e., $E_i(N) = E(N)/N$, Eq. (2.3) implies that the corresponding dipole moments also vanish, cf. (1.2a):

$$\vec{d}(N) = \sum_{i=1}^N \vec{r}_i = 0. \quad (2.4a)$$

But this is only a sufficient condition. There are many equilibrium configurations for which

$$\sum_{i=1}^N E_i(N) \vec{r}_i = \sum_{i=1}^N \vec{r}_i = 0, \quad (2.4b)$$

even though $E_i(N) \neq E_j(N)$ for at least one pair of indices. If the interaction energies of the charges are logarithmic, Eq. (2.2) is replaced by

$$\vec{F}_i = \sum_{j=1, j \neq i}^N \frac{\vec{r}_i - \vec{r}_j}{|\vec{r}_i - \vec{r}_j|^2} = \frac{1}{2} (N - 1) \vec{r}_i. \quad (2.5)$$

This expression shows that all the equilibrium forces have the same magnitude and — in analogy with (2.4b) — the corresponding dipole moments vanish identically [16]. These constraints indicate that the equilibrium configurations of the surface logarithm problem generally tend to be more regular than the equilibrium states of the surface Coulomb problem. In both cases the equilibrium coordinates \vec{r}_i satisfy sets of linear relations, such as (2.3) and (2.4b), which are vectorial generalizations of cryptographic knapsack problems: these are known to be computationally difficult, or NP - hard [52].

The locally stable equilibrium configurations of the surface Coulomb problem satisfy the additional constraint that the associated energies are local minima. Specifically, if the charge positions are described by spherical coordinates — the co-latitudes $0 \leq \phi_i \leq \pi$, and longitudes $-\pi \leq \theta_i \leq \pi$ — then the Coulomb energy (2.1) is $E(\phi_i, \theta_i)$, $1 \leq i \leq N$; and the equilibrium condition (2.2) is equivalent to

$$\frac{\partial E}{\partial \phi_i} = \frac{\partial E}{\partial \theta_i} = 0, \quad 1 \leq i \leq N. \quad (2.6a)$$

If Ω_κ , $1 \leq \kappa \leq 2N \leftrightarrow \phi_1 \dots \phi_N, \theta_1 \dots \theta_N$, then a sufficient condition for the local stability of the solutions of (2.6) is that the associated Hessian matrix

$$\mathcal{H}(\Omega_\kappa, \Omega_\mu) = \frac{\partial^2 E}{\partial \Omega_\kappa \partial \Omega_\mu}, \quad 1 \leq \kappa, \mu \leq 2N \quad (2.6b)$$

is positive definite. See Appendix A. Physically, this simply means that tangential restoring forces, i.e. $\vec{F}_i^{\text{rest}} \cdot \vec{r}_i = 0$, counter small displacements from equilibrium. In potential theory these locally stable configurations are known as Fekete points, and some asymptotic estimates of the rate of approach to the limit of continuous charge distributions are available [55, 56]. In Section 3B these methods are used to construct an expression for the ground state energy $E(N)$.

Both in the Coulomb and dipole problems analytic solutions of the equilibrium equations (2.6a) and evaluation of the associated Hessians (2.6b) becomes tedious for as few as four interacting objects [32, 57]. At present, the only practical way of surveying the locally stable states of the Coulomb systems for larger values of N is to use computers to find energy minima. However, since the number of minima appears to grow exponentially with N , the energy surface $E(\phi_1, \theta_1; \dots; \phi_N, \theta_N)$ becomes progressively more convoluted, and for $N > O(10^2)$ has many small hills and valleys. This leads to fundamental difficulties in mapping out the topography of the energy surfaces: It is necessary to distinguish genuine physical features such as minute ridges or clefts arising from the competition among the $N(N-1)/2$ charge interactions from numerical artifacts such as corrugations due to roundoff or truncation errors. Furthermore, even high statistics computer searches can miss some minima with small capture basins or special symmetries. The net result is that computer trials can both over - and underestimate the actual number of locally stable states. Analytic and numerical stability criteria for multidimensional

energy surfaces are discussed in more detail in Appendix A.

B. Computer Algorithms

Most of the numerical work was carried out with the ACPMAPS supercomputer at Fermilab. This is a parallel processing machine utilizing 600 double precision nodes. The computer searches for the locally stable states of the surface Coulomb problem were started from sets of points randomly distributed over the surface of the sphere --- specifically, 10^4 random starts for every value of N in the range $2 \leq N \leq 64$; 2000 starts for each successive N in the interval $65 \leq N \leq 108, 111$; and 1000 starts for $N = 109, 110$, and 112. The initial charge configurations were described by sets of spherical coordinates $\vec{r}_i (\phi_i, \theta_i)$, where each angle is represented by a 24-bit, or 7 decimal, pseudo-random number normalized to yield a uniform spherical distribution [19, 20]. The equilibrium states were found by allowing the points to move in the direction of the forces acting on them subject to the constraint of remaining on the surface of the sphere. The steepest descent method of iterating the map $\vec{r}_i \rightarrow \vec{r}_i' = (\vec{r}_i + \gamma \vec{F}_i) / |\vec{r}_i + \gamma \vec{F}_i|$, with γ chosen to maximize convergence, was used for this problem by Claxton and Benson [43]. In the limit $\gamma \rightarrow \infty$, the update formula reduces to $\vec{r}_i \rightarrow \vec{r}_i' = \vec{F}_i / |\vec{F}_i|$, which is an over-relaxed update step with good convergence. If this step is so large that the $\{\vec{r}_i'\}$ configuration has a higher energy than the $\{\vec{r}_i\}$ state, γ is automatically adjusted downward for that step until the energy does decrease. The iterations are terminated when the energies stabilize within the machine precision of one part in 2^{48} (~ 14.4 decimals).

Since these computations involve the cancellation of large forces it is essential to use at least 48-bit precision. Conjugate-gradient methods do not improve this technique because of the highly convoluted structure of the energy surface.

In order to compare the geometric properties of the equilibrium states it is useful to rotate the configurations into a standard set of orientations. According to (1.3) the N charges of a locally stable state may be labeled by their partial energies. Suppose that these are ordered in a non-decreasing sequence, i.e.

$$E_1(N) \leq E_2(N) \leq E_3(N) \leq \dots \leq E_N(N). \quad (2.7)$$

As a first step in orienting, pick a charge with the lowest partial energy --- if $E_1(N) = E_2(N)$, etc., this won't be a unique choice! --- and rotate the configuration so that this charge is placed at the north pole, $\theta = \phi = 0$. Consider next the set of charges with the second lowest partial energies: for instance, E_3, E_4, E_5 , if (2.7) has the special form

$$E_1 = E_2 < E_3 = E_4 = E_5 < E_6 \dots \leq E_N. \quad (2.8)$$

Find the (not necessarily unique) charge in this set closest to the north pole, and rotate the entire configuration so that this second charge is at zero longitude, $\theta = 0$. If the second charge happens to be at the south pole, repeat the process with another charge from the set with the third lowest partial energies. This scheme is adequate because the orientations are unique for

irregular configurations, and the ambiguities are irrelevant for comparing symmetric configurations.

The numerical reproducibility of the computations can be checked by comparing the results obtained from minimizing runs starting at different random initial configurations. For instance, for $N = 84$, the reproducibilities of some of the typical values that describe the characteristics of the configurations --- e.g., the chiral states with the largest capture basin --- are:

total energy	Eq. (1.3)	3103. 478 717 096	13 digits	(2.9a)
--------------	-----------	-------------------	-----------	--------

lowest partial energy	Eq. (1.3)	36. 885 477	8 digits	(2.9b)
-----------------------	-----------	-------------	----------	--------

typical angular	{	θ	0. 039 852 25	7 digits	(2.9c)
coordinates (rad.)		ϕ	0. 010 146 18	7 digits	

The disparity in significant digits between the total and partial energies is not due to statistical fluctuations or roundoff errors. Rather, it indicates that the computer runs end in a multiplicity of shallow stability valleys that merge into the local energy minima. The relation of these 'eigenmodes' to the Hessian stability criterion, Eq. (2.6b), is discussed in Appendix A. The basic numerical consequence is that the slight variations of the individual charge positions and energies compensate in such a way that the total energies of the equilibrium configurations are reproducible with a gain of five additional significant digits.

3. Locally Stable States of the Surface Coulomb Problem

A. Variation of the Number of States with the Particle Number N

The computer trials show that when there are only a few interacting charges --- that is

N is in the range $2 \leq N \leq 14$ --- the energy minimizing algorithm leads to a unique terminal energy $E(N)$ for every value of N . If the associated charge configurations are rotated into a standard orientation by means of the conventions established in Section 2B, then the resulting geometrical patterns $C(N)$ are also unique. A new level of complexity appears at $N = 15$. In this case all the computer searches still converge to a unique final energy value $E(15) = 80.67024411$; but the associated charge configurations are split into a pair of enantiomeric states: Out of a total of 10^4 randomized initial configurations 4958, or 50%, of the energy minimizing sequences terminate in a charge pattern $C^L(15)$, which is the chiral transform of another pattern $C^R(15)$ reached in the other 5042 energy minimizations.

Three distinct terminal configurations appear when $N = 16$. As indicated in Table VIII in Appendix B, 75.7% of the 10^4 minimizing runs end at an energy of $E_1(16) = 92.91165530$. The frequency of occurrence of this state, or 'capture basin', is in turn almost evenly divided (37.7% and 38.0%) between two enantiomeric configurations $C_1^L(16)$ and $C_1^R(16)$. The remaining 24.3% of the computer searches end at a locally stable state with a slightly higher energy, $E_2(16) = 92.92035396$. The associated charge configuration $C_2(16)$ is a symmetric set of four rings outlining a series of four relatively rotated squares with a charge at every corner. Figures 1(a) - 1(d) show these configurations in detail.

A summary of the multiplicities of the states $M(N)$ for all N in the range $2 \leq N \leq 112$ is given in Table I. As indicated in column two of the Table, $M(15) = 2$ and $M(16) = 3$ because every chiral configuration is counted as a separate state. Columns 3, 6, 9 and 11 also list the cumulative number of states.

$$M_c(N) = \sum_{j=2}^N M(j). \quad (3.1)$$

The graph in Figure 2 shows that $M_c(N)$ increases at an exponential rate with N . In particular, if we assume that

$$M(N) = A e^{vN} \quad (3.2a)$$

then (3.1) implies

$$M_c(N) = A(e^{vN} - e^v)/(1 - e^{-v}). \quad (3.2b)$$

A Newton-Raphson optimization shows that for $70 \leq N \leq 112$, Eq. (3.2b) provides an excellent fit of the data with

$$A = 0.382 \quad \text{and} \quad v = 0.0497. \quad (3.2c)$$

An exponential growth of the multiplicities of states is also observed in two-dimensional arrays of pivoted magnets. Extensive experiments with $n \times n$, $2 \leq n \leq 6$ systems, initially stirred by fluctuating magnetic fields, and then allowed to settle into locally stable configurations, show that the number of distinct patterns $M^n(N)$ is of the order of

$$M^n(N) \approx 1.3 e^{0.19N}, \quad (3.3)$$

where $N = n \times n$ is the number of magnets [57, 58]. Figure 2 shows that the multiplicity of the magnetic states grows much more rapidly than the multiplicity of the surface Coulomb states. This trend is plausible because the magnets are coupled by a vector interaction that generates complex domain structures.

Table I

Variation of the Number of States $M(N)$ with the Particle Number N

N	M(N)	$M_c(N)^a$	N	M(N)	$M_c(N)$	N	M(N)	$M_c(N)$	N	M(N)	$M_c(N)$
2	1		29	2		57	9		85	19	505
3	1		30	3	43	58	18		86	46	
4	1		31	1		59	9		87	39	
5	1		32	2		60	11	200	88	32	
6	1		33	1		61	13		89	37	
7	1		34	2		62	6		90	44	703
8	1		35	5	54	63	4		91	37	
9	1		36	2		64	10		92	49	
10	1	9	37	3		65	6	239	93	41	
11	1		38	2		66	4		94	55	
12	1		39	4		67	2		95	35	920
13	1		40	6	71	68	9		96	41	
14	1		41	3		69	9		97	21	
15	2	15	42	7		70	13	276	98	37	
16	3		43	1		71	7		99	24	
17	1		44	1		72	10		100	52	1095
18	1		45	3	86	73	10		101	82	
19	1		46	8		74	22		102	87	
20	1	22	47	10		75	6	331	103	52	
21	2		48	3		76	12		104	56	
22	2		49	2		77	9		105	70	1442
23	2		50	1 ^b	110	78	7		106	93	
24	2		51	3		79	7		107	86	
25	1	31	52	8		80	10	376	108	75	
26	2		53	3		81	19		109	86	
27	3		54	10		82	30		110	93	1875
28	2		55	11	145	83	31		111	88	
			56	8		84	30		112	91	2054

^a Cumulative number of states, Eq. (3.1).^b $M(N) > 1$ for $N > 50$.

There are several other N-body systems that exhibit an exponential growth of $M(N)$ with $v \sim 0.07$ and 0.16 , [59]. In these statistical models the index v is identified with a 'maximum configurational entropy', i.e.

$$v = \lim_{N \rightarrow \infty} \frac{1}{N} \ln [M(N)]. \quad (3.4)$$

If these results are combined with the trends of the surface Coulomb problem and the magnetic arrays, it is plausible to conjecture that in general the number of locally stable states of N-body cooperative systems increases exponentially with N . This conjecture has several practical consequences: If the exponential growth in the number of metastable states of the surface Coulomb problem continues to increase at the rates indicated in (3.2a) and (3.2c), then the numerical simulation of large systems $N > O(10^3)$ involves severe problems. For instance, the energy manifold describing the Coulomb interaction of 2000 charges constrained to the surface of a sphere would have about 5×10^{42} locally stable minima. Implementing numerical optimization or search algorithms and testing for stability on such an intricately corrugated energy landscape would strain current computing resources beyond their limits.

B. Energy Distributions

The electrostatic energy of the N- particle surface Coulomb problem, Eq. (2.1), is given by explicitly by

$$E(\phi_1, \theta_1; \dots; \phi_N, \theta_N) = \frac{1}{2} \sum_{i=1}^N \sum_{j>i}^N \{ \sin \phi_i \sin \phi_j \sin^2 [\frac{1}{2}(\theta_i - \theta_j)] + \sin^2 [\frac{1}{2}(\phi_i - \phi_j)] \}^{-1/2}, \quad (3.5)$$

where $\phi_i \in [0, \pi]$ and $\theta_i \in [-\pi, \pi]$ are the spherical coordinates of the i^{th} charge.

Geometrically, $E(\phi_1 \dots \theta_N)$ corresponds to a surface in a $2N + 1$ dimensional space. The highest peaks on this energy 'landscape' are generated by configurations where some of the charges are close together. The median range of heights is associated with randomly distributed sets of coordinates --- such as those used as the starting configurations for the computer searches. The lowest points of the valleys and craters correspond to locally stable configurations of the surface Coulomb problem. As indicated by (3.2a) and (3.2c), the number of these local minima increases at an exponential rate with N . Geometrical comparisons show that for a given value of $N > 1$, the charge configurations associated with these minima all tend to be quite different. Nevertheless, the relative energy variations between the lowest and highest local minima are less than 0.006% even for the largest multiplicities of states, i.e. $M(112) \approx 0.382 e^{5.56} \approx 100$.

B-1. Energies of Random Initial Configurations. Let $E_j^{\text{ran}}(N)$, $1 \leq j \leq p$, denote the energies of a set of random distributions of N charges on the surface of a unit sphere, where a total of $p > 1$ configurations are generated. Then ergodic arguments and rigorous results of potential theory [56] both show that the average energy of the set of random states is given by

$$\langle E^{Ran}(N) \rangle = \lim_{p \rightarrow \infty} \frac{1}{p} \sum_{j=1}^p E_j^{Ran}(N) = \frac{N^2}{2}, \quad (3.6)$$

where $N^2/2$ is the Coulomb energy of a continuous uniform spherical surface charge distribution with total charge N . Figure 3 and Table II show some of the results obtained from computer simulations with $p = 10^5$, and N varying throughout the range $6 \leq N \leq 100$. The overall agreement is good although the computer generated averages $\langle E^{Ran}(N) \rangle$ tend to exceed the theoretical values $N^2/2$ by about 6%. This bias is also evident in the asymmetric distribution of the maximum and minimum energy values about the mean displayed in columns 3,4 and 5 of Table II. The underlying reason is that random selections of angular coordinates include charge clusters [60], and these configurations boost the energy values in (3.5).

The computer simulations of the random charge configurations can also be checked by calculating their dipole moments, Eq. (1.2a). In an independent series of trials the 'random walk' result $\langle |\vec{d}(N)| \rangle_{Ran} = 0.9213 N^{1/2}$, cited in (1.2b), was verified by generating 100 random configurations for every value of N in the range $3 \leq N \leq 64$. Finally, by combining (1.2b) and (3.6) in the invariant ratio

$$R \equiv \frac{\langle |\vec{d}(N)| \rangle_{Ran}}{\langle E^{Ran}(N) \rangle^{1/4}} = \left[\frac{2^{7/2}}{3\pi} \right]^{1/2} = 1.095\,637, \quad (3.7)$$

it is possible to cross-check the consistency of the energy and dipole moment simulations.

The numbers listed in the last column of Table II yield an average ratio of $R = 1.110$, which is within 1.3% of the theoretical value.

B-2. Minimum Energy States. Let $E_1(N)$ denote the lowest energy states of the N-body surface Coulomb problem found by computer searches. A complete set of values, ranging from $E_1(3) = 3^{1/2} = 1.732\dots$, to $E_1(112) = 5618.04488233$, is listed in column 4 of Table VIII in Appendix B. In the absence of rigorous analytical bounds we cannot exclude the existence of other configurations with even lower energies. The sequence of crosses in Fig. 3 shows the variation of E_1 with N in graphical form. On this coarse energy scale $E_1(N)$ is a smooth monotonic function: The simple expression

$$E_{1F}(N) = 0.5N^2 - 0.5513 N^{3/2} \quad (3.8)$$

fits the data with error bounds of 0.1% at $N = 20$ and 0.01% at $N = 112$. Using $E_{1F}(N)$ as a smooth baseline, it is possible to construct scatterplots of the energy differences $E_{1F}(N) - E_1(N)$ on an enlarged scale. However, searches for systematic deviations resembling the energy peaks associated with atomic clusters [61] or analogues of Thomas-Fermi oscillations [62] have not led to any conclusive results [16, 40].

The functional form of $E_{1F}(N)$ has two physical interpretations [30]: (i) $N^2/2$ is the electrostatic energy of a uniform surface charge density — with total charge N — on a unit

Table II

Electrostatic Energies and Dipole Moments of Random Spherical Charge Distributions

N	$N^2/2^a$	$\langle E^{Ran}(N) \rangle^a$	σ^b	$Max \{E^{Ran}(N)\}$	$Min \{E^{Ran}(N)\}$	R^c
10	50	47.30	7.76	99.11	34.35	1.116
20	200	197.85	13.32	270.65	164.82	1.092
30	450	457.74	78.76	2594	395.85	1.107
40	800	835.63	198.4	3716	721.6	1.204
50	1250	1317.2	288.9	4416	1143	1.092
64	2048	2182.0	446.5	6229	1920	1.050
80	3200	3428.9	630.3	7824	3047	-
100	5000	5392.4	864.1	10 886	4851	-

^a Eq. (3.6)^b standard deviation^c Eq. (3.7)

sphere. In order to recover the energy of a distribution of N point charges it is necessary to subtract the self-energies of a set of N uniformly charged spherical caps centered on these points. For $N > 1$, it is plausible to approximate the caps by disks. Since the energy of an infinitely thin disk of charge with radius a is $E_D = 2\pi^2\sigma^2a^3 \{0.4244\}$, where σ is the charge density [63, 64]; the total self-energy correction is of the order of NE_D where $\sigma = (\pi a^2)^{-1}$.

For simplicity, suppose that all the disks have the same radius. Then the crudest measure of

the total area covered by the N disks is the surface area of a unit sphere, i.e., $N\pi a^2 = 4\pi$.

Consequently, the self-energy correction is approximately given by

$$NE_D \approx 0.4244 N^{3/2}; \quad (3.9)$$

which accounts for the second term in (3.8). More elaborate estimates that improve the agreement with the empirical coefficient 0.5513 are outlined in reference [40]. (ii) Equation (3.6) shows directly that $N^2/2$ can also be identified with the average energy of a set of N unit charges randomly distributed over the surface of a unit sphere. In this case, the $O(-N^{3/2})$ term represents the correlation energies of the ordered Coulomb equilibrium states.

B-3. Energies of Metastable States. The most striking feature of the metastable states is that their energies are closely bunched just above the minimum energy states. This trend begins with the first metastable state at $N = 16$: As indicated in column 4 of Table VIII in Appendix B, the energy difference $\Delta E(16)$ between the two states is

$$\begin{aligned} \Delta E(16) &= E_2(16) - E_1(16) \\ &= 92.920\,353\,96 - 92.911\,655\,30, \\ &= 0.008\,698\,66; \end{aligned} \quad (3.10)$$

and this implies $\Delta E(16)/E_1(16) \approx 9.36 \times 10^{-5}$. Figures 1 (a) and 1 (c) show that this small relative energy difference is not reflected in any geometric similarities between these

two states. At the other extreme, for $N = 112$, the computer searches lead to 60 locally stable states with distinct energy values --- 31 of these states occur in enantiomorphic pairs. In this case it is convenient to describe the level spacings by the average energy difference $\langle \Delta E(112) \rangle$, i.e.,

$$\begin{aligned} \langle \Delta E(112) \rangle &= [E_{60}(112) - E_1(112)]/59, \\ &= [5618.419\ 481\ 31 - 5618.044\ 882\ 23]/59, \\ &= .006\ 349\ 14; \end{aligned} \quad (3.11)$$

which indicates that the relative spacings are of the order

$$\langle \Delta E(112) \rangle / E_1(112) \approx 1.13 \times 10^{-6}.$$

In general, $\langle \Delta E(N) \rangle = [E_n(N) - E_1(N)]/(n - 1)$, for N charges, where $n (> 1)$

denotes the number of distinct energy levels. Table III shows the trends in level spacings for

Table III

Variation of the Average Energy Level Spacing $\langle \Delta E(N) \rangle$ with the Number of Charges N

N	16	21	22	27	30	32
n	2	2	2	2	2	2
$\langle \Delta E(N) \rangle$.008 70	.000 29	.020 42	.006 99	.000 45	.207 12
N	55	56	57	58	59	60
n	6	4	5	10	5	6
$\langle \Delta E(N) \rangle$.005 49	.051 22	.022 16	.013 08	.004 36	.030 07
N	107	108	109	110	111	112
n	52	47	56	59	52	60
$\langle \Delta E(N) \rangle$.007 38	.007 37	.004 94	.004 01	.007 16	.006 35

18 values of N ranging from 'small' to 'large'. Since $\langle \Delta E(N) \rangle / E_1(N) \sim 10^{-6}$ for $N > 100$, computer searches for the lowest energy states in complex systems of this type require high precision. In fact this energy scale is so fine that neither the empirical fit (3.8), nor its graph on Fig. 3, can discriminate between the ground and metastable states.

It is also interesting to display the distribution of the density of states. Table VIII shows that for $N = 112$ there are 60 states with energies spread between 5618.044 and 5618.419. If these states were distributed uniformly there would be about 8 states per bin for bins of width 0.05. With this particular choice of bin width, the first bin covers the energy interval 5618.044 to 5618.094, but according to Table VIII contains only two states. The second bin extends from 5618.094 to 5618.144, and contains no states; etc. Similarly, for $N = 111$, the first bin of width 0.05 spans the interval 5515.293 to 5515.343, and contains only the ground state; etc. The histogram in Fig. 4 shows the combined statistics for $N = 111$ and 112 — a total of 112 states. Clearly the level distribution is not uniform. There is a dip, or 'level-repulsion', in the energy bin just above the ground state; a pronounced maximum in the middle of the range; and an eventual decrease in the density of the highest levels. This density profile formally resembles the Wigner distribution of the energy level spacings of large 'random' Hamiltonian systems [65].

Figure 5 shows a semi-log plot of the density of states weighted by the probability of occurrence. It is a straightforward matter to include this additional information. Specifically, for $N = 112$, Table VIII shows that the two states falling into the first energy bin between 5618.044 and 5618.094 appeared 620 times in 1000 computer searches starting from different random configurations. On average, therefore, their relative probability of

occurrence is 62%. Similarly, for $N = 111$, the state in the first energy bin occurred in 48% of the computer trials. The combined average for these three states therefore is 55%; and this is the value indicated for the first bin in Fig. 5. The rest of the histogram can be obtained by similar means.

The most conspicuous difference between the two histograms in Figs. 4 and 5 is that the maximum of the probability density occurs near the minimum energy states. In general, this implies that for values of $N \gtrsim 100$ there is about a 95% probability that a computer search will end at an energy level within 0.003% of the ground state. But it is difficult to improve this precision. In the range $100 \leq N \leq 112$, the average probability that a computer minimization will actually reach the minimum energy state is only 35%. Of course, this result depends on the choice of minimizing algorithm. Nevertheless, similar statistical behavior occurs in the distribution of patterns in magnetic cooperative arrays [58]. All of these systems display the same basic trend: as the number of interacting objects increases, the statistical weight of the ground state decreases.

The survey of metastable states summarized in Table VIII is based on a total of about 7×10^5 computer trials. Rare states, with probabilities of occurrence as low as 0.01% are found for $N = 21, 30, 42, 48, 58$, and 61. Possibly there are additional states with still smaller capture basins. Certainly it is plausible that for $N = 112$ some states on the high energy tail of the histogram in Fig. 4 have been missed due to limited statistics (only 1000 energy minimizing searches). But the essential observation is that none of the numerical trials — for any value of N — has yet turned up any trace of isolated energy levels; that is, single levels separated by large 'band gaps' ($\gg \langle \Delta E(N) \rangle$) from the cluster of states above the ground state. It remains

to be seen whether this trend continues for still larger values of N .

B-4. Energies of Individual Charges. The total electrostatic energy of a locally stable state of N charges can be represented as the sum of the partial energies associated with the individual charges. These partial energies have two interesting properties: (1) The variation of the individual charge energies *within* a configuration is generally much larger than the variation of the total energy *between* configurations. And (2), since the energy apportioned to a charge is simply the sum of the inverse distances to all the other charges, the variation of the individual energies is a measure of the geometric regularity of the configurations. Fig. 6 illustrates some of these energy relations. Specifically, let $E_m(N)$ denote the total energy of the m^{th} state of N charges. Then a slight extension of (1.3) shows that

$$E_m(N) = \sum_{i=1}^N E_{m,i}(N); \quad E_{m,i}(N) = \frac{1}{2} \sum_{j \neq i}^N |\bar{r}_i - \bar{r}_j|^{-1}, \quad (3.12)$$

where $E_{m,i}(N)$ is the partial energy of the i^{th} charge in the m^{th} state of N objects. The scatter plot in Fig. 6 begins at $N = 16$. This entry corresponds to the following array of total and partial energies, cf. (3.10):

<p>N = 16; ground state</p> <p>Fig. 1(c) and Fig. 1(d)</p> <p>$E_1(16) = 92.911\ 655\ 30$</p> <p>$E_{1,1}(16) = 5.762\ 143\ 2$</p> <p style="text-align: center;">↓</p> <p>$E_{1,4}(16) = 5.762\ 143\ 2$</p> <p>$E_{1,5}(16) = 5.821\ 923\ 5$</p> <p style="text-align: center;">↓</p> <p>$E_{1,16}(16) = 5.821\ 923\ 5$</p>	<p>N = 16; metastable state</p> <p>Fig. 1(a) and Fig. 1(b)</p> <p>$E_2(16) = 92.920\ 353\ 96$</p> <p>$E_{2,1}(16) = 5.793\ 787\ 0$</p> <p style="text-align: center;">↓</p> <p>$E_{2,8}(16) = 5.793\ 787\ 0$</p> <p>$E_{2,9}(16) = 5.821\ 257\ 1$</p> <p style="text-align: center;">↓</p> <p>$E_{2,16}(16) = 5.821\ 257\ 1$</p>
--	--

(3.13)

The spread of partial energies in the ground state is $E_{1,16}(16) - E_{1,1}(16) = 0.059\ 780\ 3$; and in the metastable state $E_{2,16}(16) - E_{2,1}(16) = 0.027\ 470\ 1$. Consequently, the average maximum energy variation *within* these configurations is 0.043 625, whereas the total energy difference *between* the configurations is only $E_2(16) - E_1(16) = 0.008\ 698\ 66$ --- smaller by a factor of 5. This disparity is also reflected in the individual charge energies: Twelve charges in the ground state, $E_{1,5}(16)$, ..., $E_{1,16}(16)$, have greater energies than any of the charges in the metastable state!

In the general case, when there are n distinct energy levels associated with N charges, the average maximum variation of partial energies within the configurations $\langle \Delta E_{part}(N) \rangle$ is given by

$$\langle \Delta E_{part}(N) \rangle = \frac{1}{n} \sum_{m=1}^n \{E_{m,N}(N) - E_{m,1}(N)\}. \quad (3.14)$$

Table IV

Variation of the Partial Energy Differences $\langle \Delta E_{part}(N) \rangle$ Within Configurations

N	16	21	22	32	55	60	111	112
$\langle \Delta E_{part}(N) \rangle^a$.043	.055	.030	.054	.117	.098	.211	.208
$R(N)^b$	5.01	189	1.44	0.26	21.3	3.19	29.5	32.7

^a Eq. (3.14)

^b Eq. (3.15)

Table IV shows that this energy spread is a slowly increasing function of N. The differences in partial and total energies can be combined in the ratio

$$R(N) = \frac{\langle \Delta E_{part}(N) \rangle}{\langle \Delta E(N) \rangle} \sim \frac{\text{Energy Differences Within Configurations}}{\text{Energy Differences Between Configurations}} \quad (3.15)$$

which is the ordinate of the scatter plot in Fig. 6. Some representative values are also listed in Table IV. Clearly most of the points in Fig. 6 fall into the band between $5 < R(N) < 50$. This demonstrates that the scale of total energy differences between successive metastable states

is much finer than the variation of the individual charge energies. A complementary pattern is exhibited by the stabilities: Eqs. (2.9a) and (2.9b) show that the numerical reproducibilities of the total energies of the configurations generally exceed the reproducibilities of the partial energies by five orders of magnitude.

The contrast between individual and collective energies is also illustrated by the following example: Suppose that the partial energy of a charge has the value 36.935 241. Then it is easy to verify from the computer results that this charge cannot be a constituent of any locally stable state with either $N \leq 83$ or $N \geq 85$; it must belong to one of the 30 configurations with $N = 84$. However, there is no finer scale of energy rankings to help in locating this charge. Everyone of the 30 states is comprised of sets of 84 partial energies that straddle the value 36.935 241. Consequently all of these states have to be examined in detail before it can be established that 36.935 241 corresponds to $E_{10,37}(84)$ — the partial energy of the 37th charge in the 10th equilibrium state of 84 objects. This assignment is unique because all 84 partial energies in the 10th state are different, and $E_{10,37}(84) \neq E_{m,i}(84)$ for all $1 \leq i \leq 84$ and $m \neq 10$. The only remaining ambiguity is geometric: as indicated in Table VIII, $E_{10}(84)$ has two enantiomeric configurations.

Equation (3.12) shows that the partial energy of a charge is proportional to the sum of its inverse distances to all the other charges. This implies that highly symmetric equilibrium configurations that 'look alike' from every charge or vertex have unique partial energies, i.e., $E_{m,i}(N) = E_m(N)/N$ for all $1 \leq i \leq N$. Indeed, this is the case for three of the Platonic solids, the tetrahedron, octahedron (dipyramid), and icosahedron, whose vertices are the equilibrium positions of the surface Coulomb problem for $N = 4, 6$, and 12 respectively. The partial

energies are also unique for $N = 8$ and 24 , even though these configurations are not included among the standard semi-regular (Archimedean) polyhedra. Clearly, less symmetric charge distributions will have a greater variety of reciprocal distances, and this dispersion can be used as a measure of geometric irregularity analogous to the angular diversity ratio (1.1): If $n_e(N, m)$ denotes the number of distinct partial charge energies that occur in the m^{th} state of N objects, then the corresponding *energy diversity ratio* (%) is given by

$$D_e(N, m) = 100 \frac{n_e(N, m)}{N}. \quad (3.16)$$

In the range $2 \leq N \leq 112$, the computer trials yield 1248 equilibrium states with distinct energies; 806 of these states occur in enantiomorphic pairs, cf. Table I. The associated energy diversity ratios are listed in column 9 of Table VIII in Appendix B, and displayed graphically in Fig. 7. Two trends are evident: (i) $D_e(N, m)$ is a slowly increasing function of N . The first configuration that is so irregular that all of its partial charge energies are different occurs at $N = 35$; i.e., $D_e(35, 4) = 100\%$. By the time N reaches 102, 34 out of a total of 54 locally stable states have energy diversity ratios in excess of 95%. This is another confirmation of the basic trend that increasing complexity is correlated with greater geometric irregularity. (ii) Figure 7 also shows that the energy diversity ratios tend to cluster in a series of bands near 17%, 24%, 50%, 75%, and 100%. It is plausible that this regularity is connected with a deeper symmetry of the surface Coulomb problem.

4. Geometric Properties of the Surface Coulomb States

The locally stable solutions of the N -charge surface Coulomb problem are constrained solely by spherical boundary conditions and the $O(4)$ symmetry of the Coulomb interaction. The exponential growth of the multiplicity of solutions — $M(N) \sim e^{0.05N}$, Eq. (3.2a) — shows that these restrictions are compatible with a great variety of geometric structures. Only in the simplest systems is there an overlap with the criteria of strict regularity that underlie the classical theories of polygons and polyhedra [13]. For instance, the Coulomb solution for $N = 3$ corresponds to an equilateral triangle inscribed in a great circle: this is the simplest example of a *regular polygon*, i.e., a plane polygon with equal interior angles and equal sides. Similarly, *regular polyhedra* are bounded by congruent regular polygons and have congruent vertices. Only the solutions for $N = 4$ (tetrahedron), $N = 6$ (dipyramid), and $N = 12$ (icosahedron) share this high degree of symmetry. The other Platonic solids, the cube with 8 vertices, and the dodecahedron with 20 vertices, do not correspond to solutions of either the surface Coulomb or Tammes problems. The *semi-regular polyhedra* are also bounded by regular polygons with congruent vertices and edges, but the polygons do not all have to be congruent to each other. This class of objects includes the thirteen Archimedean polyhedra as well as infinite sets of semi-regular prisms and anti-prisms. None of the surface Coulomb configurations match any of these semi-regular polyhedra. In particular, the well known 'bucky ball', or truncated icosahedron, associated with C_{60} is not a solution of either the Tammes or surface Coulomb problems for $N = 60$.

Every Archimedean polyhedron has a dual formed by joining a point that is above the center of each face of the polyhedron to equivalent points above all the neighboring faces. The

lines connecting these points are constrained to intersect the edges of the original polyhedron. The resulting *duals of the semi-regular polyhedra* have congruent faces but none of these faces are regular polygons. These duals are also less symmetric than the Archimedean figures because not all of their vertices lie on a single sphere; consequently none of the dual polyhedra coincide with any of the solutions of the surface Coulomb problem [66, 67, 68]. However, there is an interesting 'near miss' for $N = 32$. The *pentakis dodecahedron* is a convex polyhedron with 32 vertices, 90 edges, and 60 faces composed of congruent isosceles triangles. This object is the dual of the truncated icosahedron which has 60 vertices and 32 faces. The two types of edges of the pentakis dodecahedron intercept angles of

$$\begin{aligned} \text{and} \quad & \sin^{-1} \left(\frac{2}{3} \right) = 0.729\ 727\ 656 \\ & \frac{1}{2} [\pi - \sin^{-1} \left(\frac{2}{3} \right) - \tan^{-1}(2)] = 0.652\ 358\ 139 \end{aligned} \quad (4.1)$$

as seen from the center of symmetry, i.e., the origin of the inter-sphere [67, 68]. These values agree to within six significant figures with the corresponding angles of the minimum energy Coulomb configuration for $N = 32$ (see the entries on lines 13 and 14 of Table V). A pictorial comparison of the pentakis polyhedron and the Coulomb configuration would show that they are essentially identical. But pentakis breaks strict spherical symmetry because its 32 vertices are distributed over two concentric spheres whose diameters differ by 2.58%. Consequently, the ratio of the two edge lengths of the pentakis dodecahedron, 1.127 322, deviates by 0.77% from the corresponding edge ratio, 1.118 600, of the Coulomb solution. In this instance, the surface Coulomb problem actually leads to a more symmetric 'dual' partner of an Archimedean

polyhedron than the original construction of pentakis by Catalan in 1862 [69]. Moreover, the minimum energy solution for $N = 32$ is not only geometrically regular, but it is also robust: in the range $12 < N \leq 65$, it is the only equilibrium configuration common to both the Coulomb and logarithmic interactions [16].

In addition to the 5 Platonic solids and 26 Archimedean polyhedra and their duals, there are only 92 other convex polyhedra whose faces are entirely composed of regular polygons --- generally not all of the same kind [17, 18]. These objects are geometrically irregular or *non-uniform* in the sense that there are no symmetry operations that transform a particular vertex into each of the other vertices in turn. Twenty-four of these non-uniform polyhedra may be inscribed in a sphere [68]. By comparing the corresponding numbers of vertices and faces it is easy to verify that none of these 24 objects match any of the surface Coulomb equilibrium configurations. In summary, therefore, out of a total of 2054 surface Coulomb states and 123 convex polyhedra derived from classical geometry, there are only three configurations common to both sets. This number is also an upper bound because further extensions of the Coulomb problem to larger systems with $N > 112$ cannot yield any additional matches. These results show that the locally stable states of complex cooperative systems of this kind tend to have symmetries that differ from those that characterize the regular polyhedral configurations of classical geometry.

A. Dipole Moments. The distribution of the dipole moments of the surface Coulomb states can be used to answer two basic questions: (1) Are the configurations for large values of N so irregular that they are approximately equivalent to random networks of points on a sphere? And furthermore, (2) do these networks approach some kind of universal asymptotic statistical

distribution that is independent of the laws of repulsion that act between the individual charges? To settle these issues, it is convenient to recall from Eq. (1.2b) that the average value of the dipole moment of a random configuration of N unit charges on a sphere is an increasing function of N , i.e., $\langle |\vec{d}(N)| \rangle_{\text{ran}} \sim N^{1/2}$. As indicated in connection with Eq. (3.7), the applicability of this 'random walk' result to the Coulomb problem can be confirmed by computer trials. In particular then for $N = 100$, the expectation value of the dipole moment of a random distribution is quite large, $\langle |\vec{d}(100)| \rangle_{\text{ran}} \approx 9.2$; whereas the entries in column 5 of Table VIII show that $0 \leq |\vec{d}(100)| \leq 0.0037$ for all 52 of the Coulomb states found by computer searches. This upper bound indicates that the metastable state with the highest energy and nearly maximal angular diversity (see below) for $N = 100$ has a dipole moment that is about 4×10^{-4} smaller than that expected for a random configuration. Figure 8 shows that this trend of small dipole moments prevails for all the Coulomb configurations in the range $N \leq 112$. The logarithmic ordinate scale of the graph extends down to 10^{-6} , which is near the limit of numerical accuracy for large systems, $N \sim O(100)$. Table VIII shows that states with vanishing dipole moments are quite common for small values of N , but tend to become less frequent as N approaches 100. Nevertheless, they don't disappear entirely: the ground state with the largest capture basin for $N = 112$ apparently has a vanishing moment. These results clearly show that the charge distributions of the surface Coulomb configurations have intrinsic regularities that persist despite the lack of the congruences or symmetries associated with the polyhedra of classical geometry.

There are systematic variations of the dipole moments that depend on the strength of the

force acting between the charges. According to Eq. (2.5), if the interaction is logarithmic, or 'soft', all locally stable configurations have vanishing dipole moments [16]. At the other extreme, the 'hard' Tammes potential, $|\vec{r}_i - \vec{r}_j|^{-n}$, $n \rightarrow \infty$, leads to states with sizable moments. Spot checks of some of the Tammes configurations found by Kottwitz's computer searches [30] yield moments larger than unity. All the available information can be summarized as follows:

<i>Force Law</i>	<i>Size of Dipole Moment</i>	<i>Source of Result</i>
$ \vec{r}_i - \vec{r}_j ^{-1}$	0	analytical identity, Eq. (2.5)
$ \vec{r}_i - \vec{r}_j ^{-2}$	$0 - 10^{-2}$	computer trials ($N \leq 112$)
$ \vec{r}_i - \vec{r}_j ^{-n}$, $n > 1$	$O(1)$	computer trials ($N \leq 90$)
random	$(8N/3\pi)^{1/2}$	combinatorial lemma, Eq. (1.2b)

Obviously, in the range $2 \leq N < O(100)$, there is no tendency for a convergence of the dipole moments associated with the logarithmic, Coulomb, or Tammes interactions. This diversity suggests the conjecture that for large values of N different force laws lead to distinct asymptotic distributions of spherical charge networks. Comparisons of trends in the Tammes and Coulomb angles (see Section 4E-1) also support this surmise.

B. Distributions of Angles. Another measure of the regularity of the surface Coulomb configurations is the *angular diversity ratio* introduced in Eq. (1.1). This has a simple basis:

If \vec{r}_i and \vec{r}_j specify the locations of two charges on the surface of a sphere with unit radius, then the set of $N(N-1)/2$ angles, $\psi_{ij} = \cos^{-1}(\vec{r}_i \cdot \vec{r}_j)$, where $\psi_{ij} \leq 180^\circ$, $1 \leq i, j \leq N$, $i \neq j$,

describes the geometry of the charge distribution. The degeneracy of this set is a measure of the symmetry of the configuration. For instance, if 5 points are distributed arbitrarily over the surface of a sphere, there will generally be $5 \times 4/2 = 10$ distinct angles between pairs of points. However, in the case of the surface Coulomb problem, the unique equilibrium arrangement of 5 charges is a triangular dipyramid — one charge at the north pole, another at the south pole, and the remaining three charges equally spaced around the equator. Obviously only three distinct angles appear between any pair of charges in this highly symmetric configuration: 180° occurs once, 120° occurs three times, and 90° occurs six times. The corresponding angular diversity ratio therefore has the low value of

$$D_a(N) = 100 \frac{\text{number of distinct angles}}{N(N-1)/2} \rightarrow 100 \frac{3}{10} = 30\% \quad (4.3)$$

Similarly, the clustering of the irregular $N = 11$ and 13 configurations around the highly symmetric icosahedron at $N = 12$ is immediately apparent from the D_a fluctuations, without the need for any graphical comparisons; viz.

N	$D_a(N)$	$D_e(N)$	$ \vec{d}(N) $	
11	36.4%	45.5%	0.0132	
12	4.5%	8.3%	0	(4.4)
13	37.2%	46.2%	0.0088	

This array shows that all three indices of regularity — the angular diversity ratio D_a , the energy diversity ratio D_e [Eq. (3.16)], and the dipole moment $|\vec{d}|$ — yield consistent results. These correlations also appear in the detailed list of values in columns 5, 9, and 10 of Table VIII in Appendix B, as well as in the graphical summaries in Fig. 9 and Fig. 10. In particular, the parallel increase of both the angular and energy diversity ratios confirms once again the general conjecture that increasing complexity tends to be associated with decreasing symmetry. For instance, the first configuration that is so irregular that all of its vertices are inequivalent ($D_e = 100\%$), and most of its edges have different lengths ($D_a = 99.2\%$) occurs at $N = 35$. Fig. 9 shows the development of this trend in graphical form. At $N = 102$, 30 out of a total of 54 locally stable states have energy and angular diversity ratios in excess of 95%. These irregularities are pervasive for $N \sim O(100)$.

The distribution of values in the sets of angles ψ_{ij} is also useful for comparing the structures of different charge configurations belonging to the same value of N . Since the data in Section 3B-3 show that the energies of all of these locally stable states are very nearly the same — within 0.007% for $N = 102$ — it is possible that some of these states also have geometrical resemblances. Well known examples of sets of complex configurations with common ‘backbones’ and minor ‘peripheral’ variations include the tautomers and conformers of structural chemistry. However, everyone of the surface Coulomb states with non-identical energies appears to have a distinct structure. For instance, at $N = 102$, there are 87 configurations (cf. Table I) each of which is described by a ψ_{ij} - set with 5151 angles.

Comparisons show that there are 33 sets that occur twice: each matching pair has the same energy and is geometrically related by an improper isometry --- evidently these are just the enantiomeric configurations. Apart from these degeneracies, there are then a total of $87 - 66/2 = 54$ different states. Further comparisons of the associated angular sets, ψ_{ij}^k , $1 \leq k \leq 54$, show that the *maximum* fraction of coincidences among any pair of these sets is bounded by 9%. Computer surveys for all N in the range $50 < N \leq 112$, where multiple states become more frequent, indicate that this overlap estimate is actually a general result; i.e., if $V(N)$ denotes the fraction of common angles, then

$$V(N) = \frac{\#(\psi_{ij}^k \cap \psi_{ij}^l)}{N(N-1)/2} \leq 0.09, \quad (4.5)$$

where $k \neq l$, and the set intersections exclude enantiomeric pairs. The low value of this overlap ratio shows that it is implausible that configurations with non-identical energies share any major structural features such as common 'backbones'.

The overlap bound in (4.5) is based on very conservative angle matching criteria. When $N \gtrsim 100$, the precision of the angular coordinates of the individual charges in rare states can decrease to about one part in 10^5 . This is degraded further by the computation of the inter-particle angle sets ψ_{ij} . Finally, the coarseness of the matching may be relaxed even more to ensure that all the enantiomeric states are correctly paired up. Consequently, the actual values of the overlap ratios $V(N)$ may be significantly smaller than the bound shown in (4.5). For

example, at $N = 84$, all 16 states with distinct energies are sufficiently irregular so that the positioning conventions of Section 2B yield unique orientations. Under these circumstances, the charge coordinates of all of these states --- which are known to 7 figures, (2.9c) --- can be compared directly. Extensive spot checks have failed to turn up even one matching charge position, apart from the common fixed point at the north pole. It seems, therefore, that the exponential increase in the number of states for larger values of $N(> 50)$ is accompanied by a tremendous proliferation of geometric structures.

C. Coulomb Polyhedra: Regular Configurations. The coexistence of order and disorder in the geometric structure of the surface Coulomb states is illustrated in Fig. 11. This diagram shows the equilibrium configuration of 19 charges on the surface of a sphere. The apparent symmetry of this arrangement is highlighted by the auxiliary polyhedron whose vertices coincide with the charge positions. The faces and edges of this polyhedron can be constructed with the help of some computer graphics: Given $N (> 3)$ points on the surface of the sphere, the set of all combinations of 3 points determines a maximum of $N(N-1)(N-2)/6$ planes. Associated with each plane and triple of points --- located by the unit vectors $\vec{r}_j, j = \alpha, \beta, \gamma$ --- is another vector \vec{r}_c extending from the center of the sphere to the plane and perpendicular to it. Since the plane and sphere intersect in a circle ($C_{\alpha\beta\gamma}$) all the scalar products $\vec{r}_c \cdot \vec{r}_j$ are equal. Suppose now that \vec{r}_k ranges over the positions of all the charges *not* included in the \vec{r}_j triplet --- i.e., the set $\{\vec{r}_\ell\}_1^N \setminus \vec{r}_\alpha, \vec{r}_\beta, \vec{r}_\gamma$ --- and furthermore that $\vec{r}_k \cdot \vec{r}_c \leq \vec{r}_j \cdot \vec{r}_c$; then the plane containing the charges α, β, γ is a face of the polyhedron. Geometrically, this inequality simply means that

the spherical cap bounded by $C_{\alpha\beta\gamma}$ contains no other charges. In cases where two or more charge triplets determine coincident planes, the associated polyhedron face is bounded by four or more vertices. Figure 11 includes an example of this situation. The end result of this construction is that the Coulomb polyhedron for $N = 19$ has a total of 33 faces. The corresponding number of edges (e) then follows from Euler's formula

$$N + f - 2 = e,$$

or

(4.6)

$$19 + 33 - 2 = 50.$$

Column 11 of Table VIII in Appendix B lists the number of faces (f) of the Coulomb polyhedra for all configurations in the range $4 \leq N \leq 112$.

The symmetries of the Coulomb polyhedron in Fig. 11 are reflected in the low values of the energy diversity, $D_e = 7/19 = 36.8\%$ [Eq. (3.16)], and the angular diversity, $D_a = 52/171 = 30.4\%$ [Eq. (4.3)]. In particular — apart from the charge at the north pole with the least partial energy — all the other 18 charges occur in pairs: each partner with the same partial energy and longitude, but the two charges differing by 180° in latitude. This symmetric pattern has a small but non-vanishing dipole moment, $|\vec{d}(19)| = 0.000\ 135$, pointing towards the north pole. The contrasting irregular features of this polyhedron arise from a lack of congruence among the edge lengths. No more than four edges have equal lengths. In fact, the 50 edges are composed of 10 groups of 4 congruent edges and 5 groups of 2 congruent edges. Consequently the polygonal faces in Fig. 11 are too irregular to fit into the standard set of non-uniform polyhedra [17,18].

A useful measure of the degree of congruence in the Coulomb polyhedra is the ratio of the number of distinct edge lengths to the total number of edges. Since the edge lengths are determined by the central angles between the corresponding vertices, this congruence measure is equivalent to a *nearest neighbor angular diversity ratio* analogous to (4.3), viz.

$$D_a^m(N) = 100 \frac{\text{number of distinct edge lengths } (\ell)}{\text{total number of edges } (e)} \quad (4.7)$$

Whereas the angular diversity D_a is a global index of the variety of all possible angles between charges, D_a^m is a strictly local measure that takes into account only the diversity of angles between adjacent charges. In the case of the $N = 19$ polyhedron, both the local and global measures of regularity yield nearly the same result

$$D_a^m(19) = 100 \times \frac{15}{50} = 30.0\% \rightarrow 30.4\% = 100 \times \frac{52}{171} = D_a(19). \quad (4.8)$$

Computer surveys of all the other Coulomb polyhedra with N vertices in the range $4 < N \leq 112$ show a similar equivalence. If this trend extends beyond $N \sim 112$, it would simplify the identification of regular charge patterns: estimates of $D_a^m(N)$ for $N > 1$ require at most the comparison of $3N$ nearest neighbor angles.

Although the dominant geometric trend of the Coulomb states is one of increasing irregularity for larger values of N , the sporadic appearance of small percentages among the

diversity ratios listed in columns 9 and 10 of Table VIII shows that some ordered patterns persist up to the limits of the computer explorations. The distribution of these special states is indicated graphically by the set of points in the 0 - 20% bands in Fig. 7 and Fig. 9. Quantitative information concerning the most regular configurations is summarized in Table V. For reference, the entries in the first line recapitulate the data for the icosahedron ($N = 12$) — the largest Platonic solid whose vertices coincide with the solutions of the logarithmic, Coulomb, and Tammes problems. Comparisons with the indices for $N = 16, 24, 32$, and 72 show that these new polyhedra are also highly symmetric. The two $N = 16$ configurations are depicted in Figs. 1(a) - 1(d): they illustrate the interesting point that the lowest energy state is not necessarily the most symmetric. Table VIII shows that this situation recurs at several other values of N ; e.g., the most symmetric $N = 82$ pattern is ranked eighth in order of increasing energy, and has an extremely low probability of occurrence. The $N = 24$ Coulomb polyhedron resembles the snub cube, one of the semi-regular Archimedean solids. However, the Coulomb interactions distort the symmetry of the classical polyhedron: Whereas the snub cube has 32 triangular and 6 square faces, all with equal edges, the faces of the Coulomb polyhedron include 24 scalene triangles [41]. The $N = 32$ situation corresponds to the 'near miss' of the pentakis dodecahedron discussed previously in connection with Eq. (4.1). In this case the Coulomb polyhedron is slightly more symmetric than its classical counterpart. The lowest energy Coulomb state for $N = 72$ is also conspicuously symmetric. All faces of this polyhedron are triangular. There is no resemblance to the aspherical $N = 72$ 'fullerene' cage containing 12 pentagons and 26 hexagons [70].

Table V
Regular Coulomb Polyhedra

N ^a	E ^b	f ^c	e/l ^d	n _e ^e	D _a ⁿⁿ (%)	Nearest neighbor angles (degrees)	Multiplicity ^f
12	49.165	20	30/1	1	3.3	63.4349 ⁱ	30
16 ^{*b}	92.911	28	42/4	2	9.5	48.9362	6
						52.5452	12
						54.6580	12
						61.8004	12
16	92.920	26	40/4	2	10.0	50.1269	8
						52.0044	8
						54.2578	16
						63.0252	8
24 [*]	223.347	38	60/3	1	5.0	42.0653	24
						45.0400	24
						45.7102	12
32	412.261	60	90/2	2	2.2	37.3773	60
						41.8103	30
72 [*]	2255.001	140	210/4	2	1.9	24.4917	60
						24.9262	30
						25.4334	60
						28.2068	60

^aNumber of charges or vertices.

^bCoulomb energy, Eq. (3.5).

^cNumber of faces, Eq. (4.6).

^dNumber of edges/distinct edge lengths, Eq. (4.7).

^eNumber of distinct partial energies, Eq. (3.16).

^fDiversity ratio, Eq. (4.7).

^gNumber of times this angle appears.

^hEnantiomeric states.

ⁱ $2 \sin^{-1} [1/2 (2 - 2/5^{1/2})^{1/2}]$.

The entries in Table V do not continue beyond $N = 72$ because the more complex symmetric polyhedra contain at least 11 different nearest neighbor angles. Nevertheless, the ordered patterns stand out clearly among the increasing variety of irregular polyhedra. For example, at $N = 112$, there are at least 60 locally stable states with distinct energies. The first, second, and tenth levels are clearly different because their nearest neighbor ratios

D_a^m [Eq. (4.7)] are 10.5%, 8.2%, and 24.1% respectively; all the other states have angular diversities exceeding 45%. The marked regularity of the second level is also apparent from the small number of partial charge energies --- equivalent to 10 types of polyhedron vertices --- and the symmetric grouping of the 330 nearest neighbor angles: these occur in 26 sets of 12 equal angles, and a residual set of 18 angles, also all alike. Unraveling the complex order of these large polyhedra is a challenging problem in 'physical' geometry.

D. Enantiomorphic Configurations. A set of points on the sphere may be transformed by *isometries* or *congruence mappings* that preserve the distances between all pairs of points. All isometries, in turn, can be built up from three basic types of transformations [71]: (i) rotations about an axis; (ii) mirror reflections in a plane; and (iii) parallel displacements of all points. If the mappings are restricted to a fixed sphere, parallel displacements play no role, and the congruence transformations reduce to *proper isometries* or (rigid body) rotations, and *rotatory reflections* composed of a reflection and a rotation whose axis is perpendicular to the mirror [13, 72]. *Central inversions*, in which the coordinates of all points are reflected in the origin of the sphere, i.e., $\vec{r} \rightarrow -\vec{r}$, are special cases of rotatory reflections in which the rotation is a half-turn.

If a pattern C_i of identical charges on the surface of a sphere is sufficiently irregular --- though not necessarily random --- then the only isometric mapping, $I: C_i \rightarrow C_f$, that yields a final configuration C_f indistinguishable from the initial state is the identity transformation. In contrast, highly symmetric configurations such as the icosahedron are invariant under a great variety of isometric transformations, e.g. the composite group $A_5 \times C_i$ [14]. The set of solutions of the surface Coulomb, logarithmic, and Tammes problems interpolates between these two extremes: In all three cases larger values of N are associated with less symmetric point groups [16, 30, 41, 42]. However, as emphasized in connection with the dipole moments in Section 4A, even Coulomb states whose only isometric symmetry is the identity transformation have ordered structures.

When $N > 50$, the surface Coulomb states tend to cluster in pairs, each with the same sequence of partial energies, equal total energy, and nearly equal probability of occurrence. Suppose that $C^L(N)$ and $C^R(N)$ denote such a pair of states. Since the orientation conventions established in Section 2B automatically include rotational degeneracies, it remains to check whether these states are related by an improper isometry. In practise, this mirror symmetry can be verified by picking a state, say $C^L(N)$, and reflecting it in an arbitrary plane through the center of the sphere. The resulting configuration is then rotated so that the charge with the lowest partial energy is positioned at the north pole, $\theta = \phi = 0$, and the charge with the next lowest partial energy is at zero longitude, $\theta = 0$. If all the partial energies are different, this orientation is unique, and the final configuration will coincide with $C^R(N)$. In case there is a

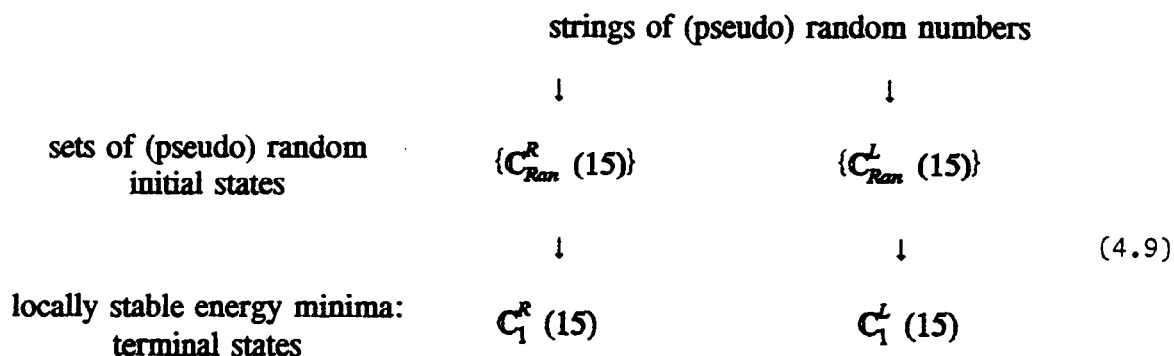
degeneracy in the partial energies, some auxiliary comparisons may be required.

The distinctions between proper and improper isometries can be illustrated with two simple examples: Figure 1(b) is a plan view of the symmetric four-ring structure of the $N = 16$ metastable Coulomb solution, $C_2(16)$. Obviously this pattern is invariant under 90° rotations and reflections — if the rings are copied on a transparency, and the transparency is flipped over, the reversed image will coincide with the original pattern. This symmetry is broken by the greater complexity of the two $N = 16$ ground states. If Fig. 1(d) is copied, the image on the flipped transparency cannot be rotated into coincidence with the original pattern, but it will match the other ground state configuration. In general, any configuration that cannot be brought into coincidence with its mirror image by rotations is *chiral* or *enantiomorphic*. Hence the familiar example of right (R) and left (L) handedness suggests the notation $C_1^R(16)$ and $C_1^L(16)$ for the two $N = 16$ chiral ground states. But for arbitrary patterns — in fact, even the simple perspective view in Fig. 1(c) — there are no obvious pictorial cues of handedness, or a ‘screw-sense’, and chirality has to be checked by other means such as exhaustive computer comparisons [73].

The asterisks in column 3 of Table VIII mark the enantiomeric states of the surface Coulomb problem. Comparisons show that $N = 15$ is the common threshold for the appearance of chiral configurations in the surface Coulomb, logarithmic, and Tammes problems [14, 16, 39]. Furthermore, in the range $15 \leq N \leq 65$, the ground states of the logarithmic potential are chiral if and only if the ground states of the associated surface Coulomb problem are chiral [16]. However, the results for $N = 15, 16, 19, 21$, etc., show that there is no such one-to-one

correspondence between the ground states of the surface Coulomb and Tammes problems [30].

There are interesting connections between chirality, 'chaos', symmetry breaking, and cryptography in the surface Coulomb problem. Let $M[C_{Ran}^R(15)] \rightarrow C_1^R(15)$ represent the mapping of a randomly chosen initial state of 15 charges, $C_{Ran}^R(15)$, to one of the pair of chiral ground states, $C_1^R(15)$ by means of an energy minimizing algorithm M . Suppose further that the initial configuration is sufficiently irregular so that it can be verified that $C_{Ran}^R(15)$ is indeed a chiral state with a mirror image $C_{Ran}^L(15)$. Then it can be shown that the minimizing algorithm of Section 2B, as implemented on a computer, preserves chirality. (An analytic analogue is discussed in [74].) This leads to an array of parallel mappings that can be extended to include many initial states:



This diagram shows that the net effect of the chirality preserving map M is to transfer the 'L' and 'R' labels from the ground states up to the level of the random initial states, and to split these into two corresponding sub-sets $\{C_{Ran}^R(15)\}$ and $\{C_{Ran}^L(15)\}$. Since the initial configurations

are distributed uniformly over the surface of the sphere, slight changes in the angular coordinates of the charges in any particular state C_{Ran}^R (15) can transform it into a C_{Ran}^L (15) state, and *vice versa*. Consequently the end result of an energy minimization can be sensitively affected by slight perturbations of the initial conditions: This mix of randomized states and unstable evolution is a basic characteristic of 'chaotic' dynamics [75].

Chiral symmetry breaking can occur in a variety of ways. For instance, varying the index n in the power law $|\vec{r}_i - \vec{r}_j|^{-n}$ can induce transitions between chiral and non-chiral states. The simplest illustration is provided by $N = 16$. In this case the ultra-repulsive Tammes potential $|\vec{r}_i - \vec{r}_j|^{-n}$, $n \rightarrow \infty$, can be approximated by choosing $n = 1\,310\,720$ [15, 30]. Both geometrical arguments [76] and computer trials then show that the $N = 16$ Tammes solution is a symmetric four-ring structure closely resembling the pattern in Figs. 1(a) and 1(b). (The latitudes of the rings are $\pm 13.632^\circ$ and $\pm 51.490^\circ$ in the Tammes case, and $\pm 11.342^\circ$ and $\pm 51.684^\circ$ in the Coulomb case.) But the lowest energy solution for the surface Coulomb problem is quite different: It is split into a pair of chiral states one of which is shown in Figs. 1(c) and 1(d). Evidently then, as the potential index n decreases from 1 310 720 to 1, there must be at least one threshold where chiral states appear.

The chiral 'L' and 'R' indices are equivalent to a binary alphabet. In principle, therefore, it is possible to construct any desired string or 'message' with an appropriate series of C_1^R (15) and C_1^L (15) configurations. But as (4.9) shows, each ground state configuration can be enciphered in an enormous number of ways by the mappings $M [\{ C_{Ran}^{R,L} (15) \}] \rightarrow C_1^{R,L} (15)$.

For instance, on a double precision computer, the number of initial states with a particular chirality can easily exceed 10^{10} . The element of ambiguity or concealment then lies in the assignment of a specific 'L' or 'R' label to any one of these random initial states. Although it is easy to verify that a particular state is chiral, the spatial arrangement of charges is usually too complex to exhibit an obvious 'handedness' --- it is necessary to go through an explicit energy minimizing sequence leading to either C_1^R (15) or C_1^L (15) in order to identify whether an initial state is 'L' or 'R'.

The strings of random numbers in the top line of (4.9) refer to the angular positions of the charges in the initial configurations. In particular, if the latitudes and longitudes of the charges are specified to an accuracy of 12 decimals, then the configurations $C_{Ran}^{R,L}$ (15) can be represented by strings of $15 \times 2 \times 12$ nominally random digits, $\{d_j\}_1^{360}$, $d_j = 0, 1, \dots, 9$. The security of this 'chiral-energy' encipherment therefore relies both on the algorithmic complexity of the mapping M and the tremendous redundancy of the correspondence

$$C_{Ran}^{R,L} (15) \leftrightarrow \{d_j\}_1^{360} \rightarrow R \text{ or } L. \quad (4.10)$$

In analogy with other schemes involving 'trap-door' or 'one-way' functions [77], eq. (4.10) is hard to invert because the reversion is a *set-valued* function that associates an entire set with a particular input [78].

In practice, the charge coordinates of the initial configurations are derived from deterministic pseudo-random number generators. The complete sequence of the chiral-energy

encipherment is therefore a combination of (4.9) and (4.10), i.e.,

$$\begin{array}{l} \text{pseudo-random} \\ \text{number generator} \end{array} \rightarrow \{d_j\}_1^{360} \rightsquigarrow C_{Ram}^{R,L}(15): M[C_{Ram}^{R,L}(15)] \rightarrow C_1^{R,L}(15) \rightarrow R \text{ or } L. \quad (4.11)$$

Since the number generators can be programmed to produce any sequence, Eq. (4.11) is a slow but feasible means of encipherment.

The concealed propagation of order through pseudo-random numbers and geometric complexity also adds a novel twist to the problem of chiral bias. This concerns the observation that naturally occurring proteins are almost exclusively composed of chiral amino acids of the 'L' variety [24, 25]. Although these compounds are far more complex than the surface Coulomb states, the basic production mechanisms are presumed to be similar in both cases: The underlying idealization is that a uniform statistical mix of initial states evolves towards equilibrium in a symmetric pair of potential wells whose minima correspond to states of opposite chirality. Since processes of this kind always lead to a racemic mix of final states, the observed 'handedness' of the biosphere is usually attributed to a critical fluctuation ('spontaneous' symmetry breaking), or a fundamental chiral force (*e.g.*, β - decay) that introduces an asymmetry in the potential wells [24, 25]. Equation (4.11) indicates still another possibility: that the final chirality is actually predetermined by a set of algorithmic instructions at a non-geometric level. It is certainly feasible to generate long strings of pseudo-random numbers that will consistently produce 'L'-handed initial configurations [23]. The appearance of a racemic or unbiased mix of initial states is therefore an illusion — the 'L' - die has already been cast

before the game begins.

The binary code of chirality disappears when (4.11) is rewritten for 14 charges. The essential difference in this case is that the ground state is not enantiomorphic even though the pseudo-random initial configurations may be chiral, i.e.,

$$\begin{array}{l} \text{pseudo-random} \\ \text{number generator} \end{array} \rightarrow \{d_j\}_1^{336} \leftrightarrow C_{Ran}^{RL}(14): M[C_{Ran}^{RL}(14)] = C_1(14). \quad (4.12)$$

The transition from (4.12) to (4.11) illustrates another threshold of structural complexity. When there are 15 charges represented by 30 blocks of 12 digit numbers — as in Eq. (4.10) — each string of 360 digits specifies a unique dichotomic variable, an 'L' or an 'R'. However, if the strings are parsed differently — as in Eq. (4.12) — they are too simple to generate the chiral alphabet. By this means the threshold of a geometric property is expressed as a minimum complexity requirement for a coding algorithm.

E-1. Coulomb Angles and Tammes Angles. The Tammes problem is equivalent to finding the largest angular diameter $\Theta_T(N)$ of N congruent caps that can be packed on the surface of a sphere without overlapping [12-14]. Column 7 of Table VIII lists the optimum values of $\Theta_T(N)$ obtained by Kottwitz [30] and Tarnai [79] for $3 \leq N \leq 100$. Clearly, $\Theta_T(N)$ is a (not strictly) decreasing function of N , with an asymptotic dependence $\Theta_T(N) \sim (8\pi/3^{1/2}N)^{1/2}$, for $N \gg 1$. There is an analogous angle for the surface Coulomb problem $\Theta_c(N)$ determined by the minimum angular separation between neighboring charges in

a locally stable configuration [39]. Several examples are contained in column 7 of Table V: $\Theta_c(16) = 48.9362^\circ$, $\Theta_c(24) = 42.0653^\circ$, $\Theta_c(32) = 37.3773^\circ$, etc. A comprehensive survey is given in column 6 of Table VIII. Since the optimization in the surface Coulomb problem is carried out with respect to total energy rather than nearest neighbor separations, the two sets of angles are related by $\Theta_T(N) > \Theta_c(N)$ when $N > 6$, $N \neq 12$. $\Theta_c(N)$ is a non-monotonic but generally decreasing function of N with an asymptotic estimate resembling the Tammes result; $\Theta_c(N) \sim (4\pi/N)^{1/2}$, for $N \gg 1$. If this estimate were accurate to leading order in N , then the relative difference between the two sets of angles would approach a constant value for large N ,

$$[\Theta_T(N) - \Theta_c(N)]/\Theta_T(N) \rightarrow 1 - 3^{1/4}/2^{1/2} \sim 0.07, N \gg 1. \quad (4.13)$$

Figure 12 shows this relative difference in graphical form when $\Theta_c(N)$ is averaged over all locally stable states belonging to a given value of N . Despite the prominent fluctuations, the overall trend is roughly consistent with (4.13).

The basic purpose of these comparisons is to see whether the configurations of points have some kind of asymptotic regularity for large values of N that is insensitive to the precise nature of the underlying interactions. If the trends in Fig. 12 can be extrapolated beyond $N \sim 112$, then it would be an indication that the local equilibrium states of the Coulomb law $|\vec{r}_i - \vec{r}_j|^{-2}$ and the Tammes interaction $|\vec{r}_i - \vec{r}_j|^{-1.310720}$ retain a distinct character even for arbitrarily large values of N .